scientific reports

Check for updates

OPEN

Assessing the detection of floating plastic litter with advanced remote sensing technologies in a hydrodynamic test facility

A. de Fockert[1]✉, M. A. Eleveld[1,2], W. Bakker[1], J. M. Felício[3,4], T. S. Costa[3], M. Vala[3], P. Marques[5], N. Leonor[3,6], A. Moreira[3], J. R. Costa[3,7], R. F. S. Caldeirinha[3,6], S. A. Matos[3,7], C. A. Fernandes[3], N. Fonseca[8], M.D. Simpson[9], A. Marino[9], E. Gandini[8], A. Camps[10,11], A. Perez-Portero[10], A. Gonga[10], O. Burggraaff[12], S. P. Garaba[13], M.S. Salama[14], Q. Xiao[15], R. Calvert[2,16], T. S. van den Bremer[2,15] & P. de Maagt[8]

Remote sensing technologies have the potential to support monitoring of floating plastic litter in aquatic environments. An experimental campaign was carried out in a large-scale hydrodynamic test facility to explore the detectability of floating plastics in ocean waves, comparing and contrasting different microwave and optical remote sensing technologies. The extensive experiments revealed that detection of plastics was feasible with microwave measurement techniques using X and Ku-bands with VV polarization at a plastic threshold concentration of 1 item/m^2 or 1–10 g/m^2. The optical measurements further revealed that spectral and polarization properties in the visible and infrared spectrum had diagnostic information unique to the floating plastics. This assessment presents a crucial step towards enabling the detection of aquatic plastics using advanced remote sensing technologies. We demonstrate that remote sensing has the potential for global targeting of plastic litter hotspots, which is needed for supporting effective clean-up efforts and scientific evidence-based policy making.

Pollution by plastic litter of the aquatic environment (oceans, seas, lakes and rivers) is a major societal and environmental problem in the Anthropocene[1,2]. After World War II, plastics rapidly became one of the most important materials used in industrial and consumer goods production worldwide. The downside of the increased use of plastics is the subsequent increase in environmental pollution due to increased waste production and mismanagement. Wind and water flows cause plastics to accumulate in the aquatic environment. When plastic pollution ends up in the marine environment, it can be found anywhere, ranging from beaches and shorelines to ocean gyres and from the equator to the poles[3,4].

Aquatic plastics primarily originate from mismanagement of waste or inflow from land[5,6]. When present in the aquatic environment, buoyant plastics are transported from rivers to seas, with some ending up in the ocean gyres[7]. During transport, larger plastic items weather due to sunlight, temperature variations, oxidative breakdown and due to enzymes present in biofilms on plastics[8]. During this weathering process microplastics

[1]Deltares, Delft 2600 MH, The Netherlands. [2]Faculty of Civil Engineering and Geosciences, Delft University of Technology, Delft 2628 CD, The Netherlands. [3]Instituto de Telecomunicações, Instituto Superior Técnico, Lisbon, Portugal. [4]Centro de Investigação Naval, Escola Naval, Almada, Portugal. [5]Instituto Superior de Engenharia de Lisboa, Lisbon, Portugal. [6]School of Technology and Management, Polytechnic Institute of Leiria, Leiria, Portugal. [7]Departamento de Ciências e Tecnologias da Informação, Instituto Universitário de Lisboa (ISCTE-IUL), Lisbon, Portugal. [8]Antenna and Sub-Millimeter Wave Section, European Space Agency (ESA), Noordwijk 2200 AG, The Netherlands. [9]Faculty of Natural Sciences, University of Stirling, Stirling FK9 4LA, UK. [10]Dept. Teoria del Senyal i Comunicacions, CommSensLab-UPC, Universitat Politècnica de Catalunya, and Institut d'Estudis Espacials de Catalunya/CTE-UPC, Barcelona 08034, Spain. [11]UAE University, Al Ain, Abu Dhabi, UAE. [12]Leiden Observatory and Institute of Environmental Sciences (CML), Leiden University, Leiden, The Netherlands. [13]Marine Sensor Systems Group, Institute for Chemistry and Biology of the Marine Environment, Carl von Ossietzky Universität Oldenburg, Schleusenstraße 1, 26382 Wilhelmshaven, Germany. [14]Faculty of Geo-Information Science and Earth Observation (ITC), Twente University, Enschede, The Netherlands. [15]Department of Engineering Science, University of Oxford, Oxford OX1 3PJ, UK. [16]School of Engineering, University of Edinburgh, Edinburgh EH9 3FB, Scotland, UK. ✉email: anton.defockert@deltares.nl

(< 5 mm diameter) are created. These microplastics are sometimes mistaken for food and consumed by aquatic life, including different fish species and mammals[8–11]. Besides consumption, entanglement by macroplastics and fishing nets is a big risk for sea life[12,13]. Plastics have been found at different depths within the water column[14], as they sink or float depending on their composition, water depth and flow velocity[15]. Sinking of plastics that would normally float can also be attributed to the development of biofilms and trapped minerals[16]. Overall, megatons of plastics are present in the upper 200 m of the oceans[17]. Of the floating plastics in the upper 5 m of the water column in the ocean, most plastics are found near the surface[18]. The observed concentrations vary significantly, reaching mass concentrations of up to 100 kg·km^{-2} in ocean gyres[7,19–21] and number concentrations ranging from 0 to 600 items·km^{-2} for items larger than 2 cm[22].

A significant mismatch exists between the estimated amount of land-generated plastic entering coastal waters (5–13 million tons per year)[5] and the estimated total amount of plastic floating at sea (less than 0.3 million tons per year)[19,23,24]. Similarly, the amount of plastics measured at sea[2,25,26] has not kept pace with growth in global plastic production[27]. To understand this mismatch, an improved understanding of the physical processes governing transport and dispersion is required[6,23,28].

All types of plastics are found in the oceans. From beach litter surveys and clean-up campaigns, lists of the most common plastic items have been compiled[29], which provide a good overview of the most common types of plastics found in the aquatic environment. The polymer with the highest relative abundance in the aquatic environment (including, freshwater systems and coastlines) is polyethylene (as high-density or low-density polyethylene, HDPE or LDPE), followed by polypropylene (PP) and polystyrene (PS)[17,30,31].

Monitoring of plastic pollution is often carried out through surveys and clean-up campaigns of beaches and net measurements in the aquatic environment[32,33]. The key limitation of these types of measurements is their limited spatial coverage. Remote sensing could play a key role in complementing existing datasets, since it can cover large areas, often the entire globe at a specific time interval. Recurring measurement enables the monitoring of developments of plastic distributions over time. Remote sensing of floating plastics has been explored using optical sensors covering the visible, shortwave to longwave infrared spectrum[34–40]. A recent review has highlighted some of the milestones[41], emphasizing the need for more research and integrated and harmonized solutions for monitoring plastic litter, as was previously suggested[42,43]. In general, natural water strongly absorbs light in the infrared region. Hence, it is considered an optically dark target. When floating plastics appear in a region of interest of a calm ocean, they would become the bright target, making it relatively easy to detect these objects[44]. However, the opacity and possible submersion of the plastics becomes a challenge for optical remote sensing technologies[45,46], which could be remedied through combination with other technologies.

Another challenge is that even in garbage patches, oceanic floating debris covers only a very small fraction of the 10 m to 1 km pixel footprints of the monitoring satellite. Microwave remote sensing, such as Synthetic Aperture Radar (SAR) imaging, has not been applied routinely to detect plastic litter in the aquatic environment[47–52]. Because radar and optical remote sensing apply different sensing techniques[53], both technologies can be complementary for plastic monitoring. SAR sensors can collect observations of surface roughness regardless of the time of day and are hardly impacted by cloud cover, whereas optical techniques capture the spectral response to solar illumination by plastics and do not work in the presence of cloud cover.

This article describes the first step towards investigating the applicability of remote sensing to the detection of floating macroplastic litter in the aquatic environment as part of European Space Agency's Discovery Campaign programme. In this first step, a variety of measurements using different microwave frequencies and visible-infrared wavelengths were conducted for different ocean wave conditions in the Atlantic Basin at Deltares (a large-scale hydrodynamic test facility, in which ocean flows and waves can be reproduced at scale). The measurements are carried out in a controlled environment, where repeatable wave conditions were used. Although important in the real ocean, we do not examine the effect of wind, as the effects of wind are harder to recreate in a reproduceable way in the laboratory and would lead to a non-homogenous (i.e., developing in space) wave field, which would make the comparison between different technologies (physically located in different parts of the basin), which is the primary objective of this paper, challenging. The radar experiments, using polarimetric microwave techniques from L-band up to K-band (1–20 GHz), were used to determine the optimum frequency and detection thresholds for various floating plastic objects under different ocean wave conditions. The aim of the optical experiments was to measure the effect of floating litter on the surface reflectance and determine whether spectro(polari)metry may be used to detect it. In our article, we focus on comparing and contrasting a number of different microwave and optical remote sensing technologies. In doing so, our objective is to explore their synergies and the potential to improve detection of plastics through a combined set of sensors.

Methods

The experiments were conducted in the Atlantic Basin at Deltares, the Netherlands, which is an 8.7 m wide, 75 m long and 1.3 m deep combined current and wave basin (the effect of currents was not explored in this campaign). The microwave and optical setups were placed on the wooden walking bridges above the facility at about 8 m above the water surface and on the yellow bridge at 1 m above the water surface, and along the sides of the basin (see Supplementary Material for locations of instrumentation).

The signal response of microwave measurement techniques and optical instruments was measured for 16 plastic items in a laboratory test facility for 3 deep-water wave conditions ($kd = 2.8$, with "k" wave number and "d" the water depth) based on a random sea with an underlying JONSWAP spectrum with different significant wave heights ($Hs = 5$, 9 and 17 cm) and wave steepness, all chosen to represent realistic ocean conditions.

The wave conditions were representative of the real ocean in the sense that the Froude number, non-dimensional water depth, spectral shape and steepness of the waves (and therefore the number of breaking waves) are similar to those in the ocean, as is common in hydrodynamic experiments involving waves (see Supplementary Information for details). Due to the much smaller size (i.e., both wavelength and wave amplitude)

of our waves in an absolute sense, the Reynolds number in our experiments is much smaller than in the field, and we do not correctly reproduce the near-surface boundary layer or any wave-driven mixing therein. Wave breaking and associated white-capping are correctly represented, as these depend on wave steepness.

The absence of wind our experiments results in the high-frequency (i.e., capillary-wave-dominated) part of the surface wave spectrum not necessarily being representative of the real ocean. As we chose to carry our experiments with real litter or similar-size plastic items, the ratio of the litter size to the microwave wavelength is comparable to the field. Compared to the wavelength of the surface gravity waves, our litter is much too large. This is a compromise we cannot avoid, and we have minimized by choosing a basin as large as possible.

During the campaign, plastics type, concentration, and size as well as water-wave conditions were varied. Measurements were carried out with optical and microwave remote sensing techniques, as listed in Table 1. Details of the instrumentation setup and the plastics used can be found in the Supplementary Material.

In addition to the microwave and optical measurements, in-situ water wave measurements were carried out using wave gauges with a frequency up to 20 Hz and optical measurements with a high-resolution camera to determine the plastic concentration at the measurement location.

The measurement duration was 15 min for each test. During the tests, different types of plastics were supplied to the basin in different concentrations; these moved towards and then through the measurement areas due to the Stokes drift associated with the waves. As the technologies used by ITP and UoS might interfere (see Table 1), these institutes always measured in sequence for the same test conditions.

Microwave measurements

Multiple microwave measurement technologies were applied (Table 1). ITP applied two separate setups corresponding to different locations of the antennas and equipment near the basin[54], with different viewing angles, frequency scanning intervals, frequency points, sweep times etc. The three antennas of setup 1 were spaced at a distance of 1 m (one dual-polarization QRH20E antenna and two V-polarized DRH30 antennas) and were directed in the direction of the wave propagation. The gain of the antennas is frequency-dependent and ranges from 6 dBi to 14 dBi across the band of 2.5–20 GHz. Setup 2 was positioned at 9 m above the water corresponding better to a satellite viewing angle. This setup involved a single V-pol, 12 dBi to 22 dBi (2.5–11.5 GHz) reflector antenna, operating in pure back-scatter mode, connected to an Agilent E5071C VNA.

The C-band Quadpol and the X-band at VV polarization was used by UoS[55]. The measuring equipment consisted of a ground-radar connected to an Anritsu Site Master S820e Vector Network Analyser, which was connected to C- and X-band antennas. The sweeps in frequency considered 1 GHz (for each band).

The GNSS-R reflectometry technique has been applied by UPC[56]. During the preparatory activities of the experiment, a GPS-like signal was generated at L1-band (1575.42 MHz) using a SMU-200 A vector signal generator. The signal power level was − 81 dBm so that it could be measured with high SNR GNSS-R observables with very short integration times (coherent integration time of 1 ms and no incoherent averaging). To track any frequency offset and drifts, a CW beacon centred at L1-band + 500 kHz was transmitted at the beginning and at the end of each GPS-like signal. Thus, the final synthesized transmitted signal consisted of 20 s of a synchronization CW beacon, followed by 40 s of an L1-band GPS signal, and finally 20 s of the synchronization CW beacon.

The research institutes used different statistical analysis methods to determine whether plastics could be detected. This is further described in the Supplementary Material.

Optical measurements

Optical detection of floating plastics was also investigated using a set of spectropolarimeters with single and multi-pixel optical sensors. A single-pixel portable ASD spectrometer and a linear spectropolarimeter GroundSPEX[58] were installed to monitor the same target to measure the above-water total radiance and the linear polarization Stokes terms. These measurements were further complemented with the FLIR BlackFly (RGB) polarisation multi-pixel imaging camera. Based on those three instruments, visible-NIR linear spectropolarimetric optical characteristics were analysed for the different plastic and wave conditions.

The ASD measurements were mostly recorded under the illumination of overhead fluorescent lamps in combination with a HPL halogen tungsten lamp. The difference in shape between the spectra of the water surface with and without floating plastics was assessed using linear regression coefficients, correlation coefficients and

		Microwave technology			Optical technology		
Institute (Country), abbrev.		Band	Frequency	Polari-sation	Instrument	Specs	Ref.
Inst. Telecom. (PT)	ITP	S - K	2–20 GHz (2 GHz bandwidth)	VV			54
Uni. Stirling (GB-SCT)	UoS	C	5–6 GHz	Quad pol			55
		X	9.5–10.5 GHz	VV			
Uni. Politècnica de Catalunya (ES)	UPC	L1 (GNSS-R)	1.5–1.7 GHz	LHCP / RHCP			56
ITC Twente (NL)	ITC				ASD	300 –2500 nm	
Uni. Oldenburg (DE) / Uni. Leiden (NL)	UoO/L				RGB camera	5 MP	57
					GroundSPEX		

Table 1. Microwave and optical sensor technologies applied in the measurement campaign.

singular value decomposition condition numbers. The degree of polarization was analysed for GroundSPEX and the RGB camera, as many types of floating plastic litter were found to impart a measurable degree of polarization ($0.05 \leq \text{DoLP} \leq 0.20$) on reflected light, making polarimetry a useful addition to a marine observing system[59].

Results

Dedicated tests were carried out to assess if the supplied plastics had a measurable (< 20 Hz) effect on the water waves. The effect of the plastics on the gravity part of the water wave spectrum (< 20 Hz) was negligible and could not be detected in the water-wave signal measured by the wave gauges for the applied concentrations, which corresponds to earlier observations[60]. The results of these measurements are further described in the supplementary material. In the subsections below, the results of the microwave and optical measurements are presented.

Microwave sensor technologies

Microwave signals reflect on the water surface due to the dielectric contrast between air ($\varepsilon_r \sim 1$) and water ($\varepsilon_r \sim 70$–80) enabling the characterization of the water surface. Floating plastics affect the water surface roughness and could therefore potentially be detected. However, the physical mechanism for the increased backscatter is still unclear. Scattering by floating plastics depends on factors such as shape, roughness caused by the indentation of the water surface, size and the value of the dielectric constant. Figure 1 illustrates the scattering mechanisms for plastics. When the water is static, the signals are reflected at a single point, as shown in Fig. 1a-I, resulting in a low backscatter intensity due to the direction of the reflected waves. If the water surface is dynamic, the signal is scattered at multiple points on the water surface, which results in an increase in backscattering. The roughness of the water surface is also increased by the indentation created by the plastic objects (Fig. 1a-III), which enables their detection using microwaves. Another scattering mechanism originates from the dielectric constant contrast between air and plastic or due to the wetted surfaces of the plastics (Fig. 1a-II). However, as the dielectric contrast between air and plastic is low, this effect is likely negligible compared to the scattering by the water surface itself. Finally, as plastic objects float, they interact with the (gravity-driven) water waves, which can cause small ripples (capillary waves) around the plastics (Fig. 1b-IV). Although the physical mechanism for increased scattering is not determined in this measurement campaign, the detection of a large variety of plastic items due to increased scattering is discussed. We begin by analysing the backscatter for the three microwave technologies in Table 1 one by one, before assessing overall detectability of different types of plastics at different concentrations in ocean wave conditions for all the microwave sensor technologies examined.

S to K-band microwaves

The energy ratio (EnR), defined as the level of scattering by the water surface including plastic litter relative to the scattering by the water surface without plastic litter has been estimated for S- up to K-band[54]. When the EnR parameter exceeds the minimum threshold value, the amount of backscattering is considered significant, which means that plastics were detected. The threshold value is defined as the average energy scattered from a reference measurement without litter (see ref 54). In Fig. 2, the backscattering results are shown for three detected plastics at a concentration of 10 g/m^2 with $Hs = 9$ cm for respectively, (a) foam cylinders, (b) plastic bottles and (c) plastic spheres. The horizontal axis shows the distance from the antenna and the vertical axis shows the successive samples at a sampling time interval of 0.8 s. The higher intensity yellow trails in the figures represent the travelling speed of individual floating objects. The trails of the foam cylinders (a) and the plastic spheres (c) correspond to the Stokes drift velocity (1.2 cm/s at a mean wave height of 5.8 cm), with which small particles are transported by waves[61–63], while the plastic bottles (b) appear to have a lower drift velocity than the theoretical Stokes drift velocity. This could be due to the deeper submergence of the bottles compared to the

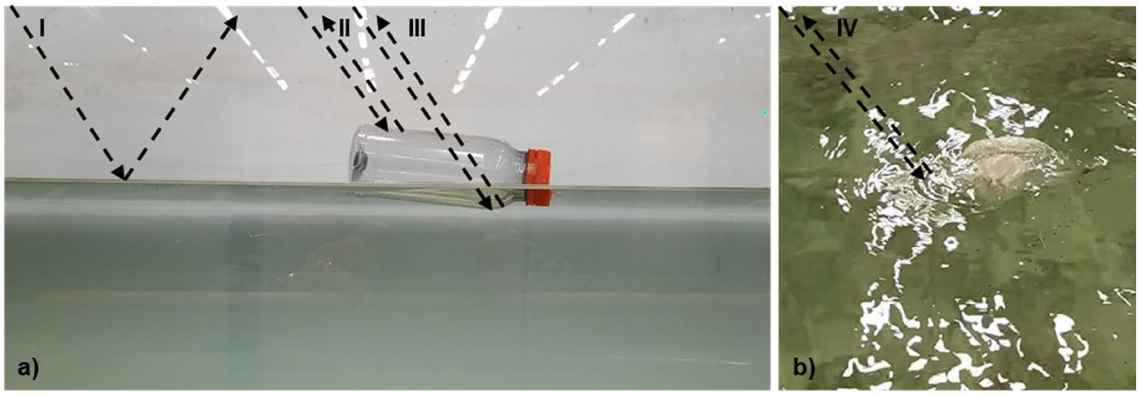


Fig. 1. Principles of different backscatter mechanisms (I-IV): (**a**) I: scattering on a flat-water surface, II: change in backscatter due to change in the dielectric constant from the (wetted) plastic items, III: change in backscatter due to indentation of the water surface. (**b**) IV: change in backscatter due to capillary waves around plastic items.

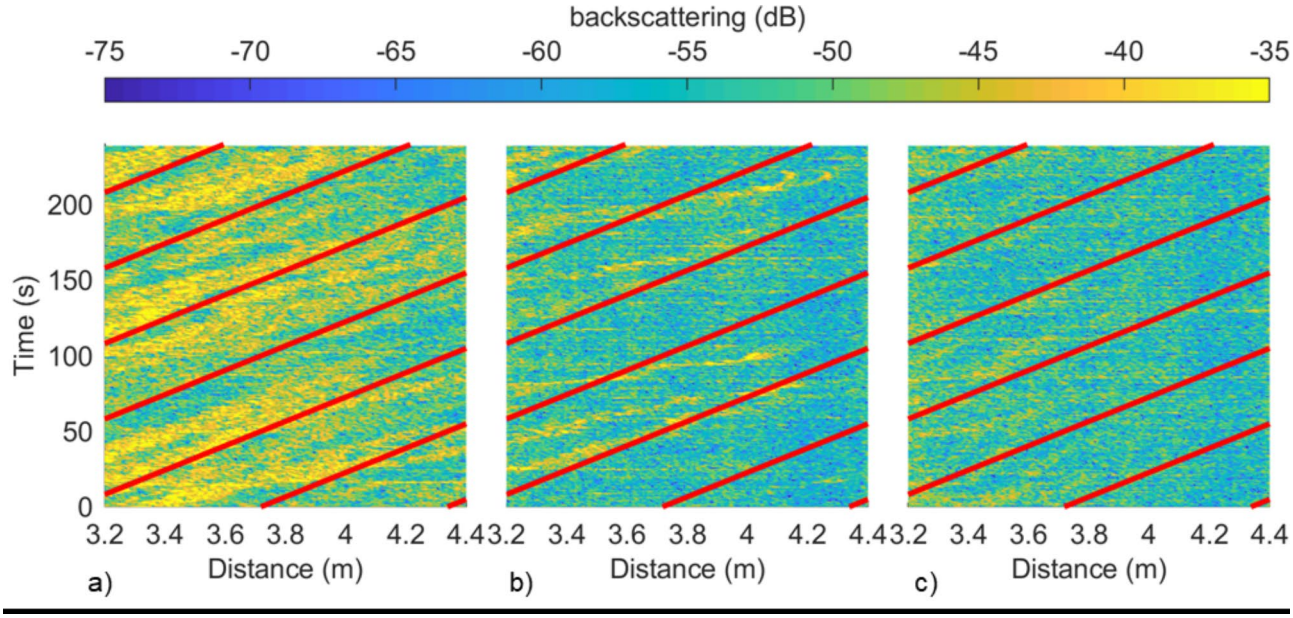


Fig. 2. Microwave backscattering at Hs = 9 cm for a concentration of 10 g/m^2 and a microwave frequency range between 2–20 GHz (S to K-bands) at VV polarization for (**a**) 5 cm length foam cylinders, (**b**) plastic bottles, (**c**) plastic spheres. The red lines in the graphs represents the theoretical Stokes drift velocity of 1.2 cm/s for a mean wave height of 5.8 cm (equals Hs = 9 cm). Because the slope of the backscattering trails in panel (**b**) is lower than the theoretical Stokes drift velocity, the plastic bottles appear to be drifting slower than the foam cylinders (**a**) and the spheres (**c**).

foam cylinders and the plastic spheres. The level of backscattering is significantly higher for the foam cylinders than for the plastic bottles and spheres.

C and X-band microwaves

The backscattering of the C- and X-band microwaves using different polarizations is shown in the intensity plots in Fig. 3. The microwave signal reflects on the water surface at 8 to 10 m from the antenna, which is shown by the grey box. Figure 3b shows the difference between the baseline situation without plastics present and with the addition of 153 g/m^2 of plastic spheres. The intensity increase for the C-band measurements is of the order of 1 dB, while a difference of 7.7 dB was found for X-band at VV polarization. The intensity peaks of up to 30 dB are from the bridge below the setup, acting as a stable reflector for the measurement signal, and can thus be ignored.

L1-band microwaves (GNSS-R)

The plastics could not be detected directly from increased scattering power[56] using the GNSS-R technique (L1-band microwaves). Even with the sensitivity of the system used (< 0.02 dB), with plastic litter in the middle of the Fresnel zone on a flat-water surface, the amount of forward scatter was too small to detect the plastics. However, the plastics could be detected by analysing the statistical descriptors of the distribution of the scattering signals. The difference is mainly observed in the standard deviation and the kurtosis of the statistical descriptors. The scattering signal and the difference in statistical parameters for litter at *Hs* = 9 cm is shown in Fig. 4. This figure shows a difference in standard deviation for a transmitted signal at right-hand central polarization (RHCP) and the receipt at left-hand central polarisation (LHCP) of 2.0 dB.

Overview microwave sensor technologies

The detectability for all test conditions for the measurements using different microwave frequencies and polarizations is shown in Table 2. Increased scattering magnitude was mainly measured for the microwave measurements from C-band up to K-band frequencies. The detectability at C-band was easier at a bandwidth of 2 GHz than for a bandwidth of 1 GHz (i.e., at half the resolution). Increased scattering was found at C-Band in 20–24% (1 GHz bandwidth) and 52–71% (2 GHz bandwidth) of the tested conditions. This increased for X-band to 72–77% and for Ku-band (12–15 Hz) to 83% of the tested conditions. We will discuss the detectability of the different plastic items in Table 2 further for different frequency bands as well as a detectability concentration threshold.

We will now discuss the main observations from Table 2 focussing on wave height, frequency band, plastic length and finally considering plastic type.

At higher wave heights, it was sometimes more challenging to detect the plastics due to wave breaking of individual waves and because the plastic items travelled faster through the footprint of the antennas due to the higher Stokes drift velocity. This is clearly seen for the detection of spheres, where all spheres were detected at a *Hs* of 5 and 9 cm for concentrations higher than 6.4 g/m^2, while the spheres could only be detected at *Hs* of 17 cm

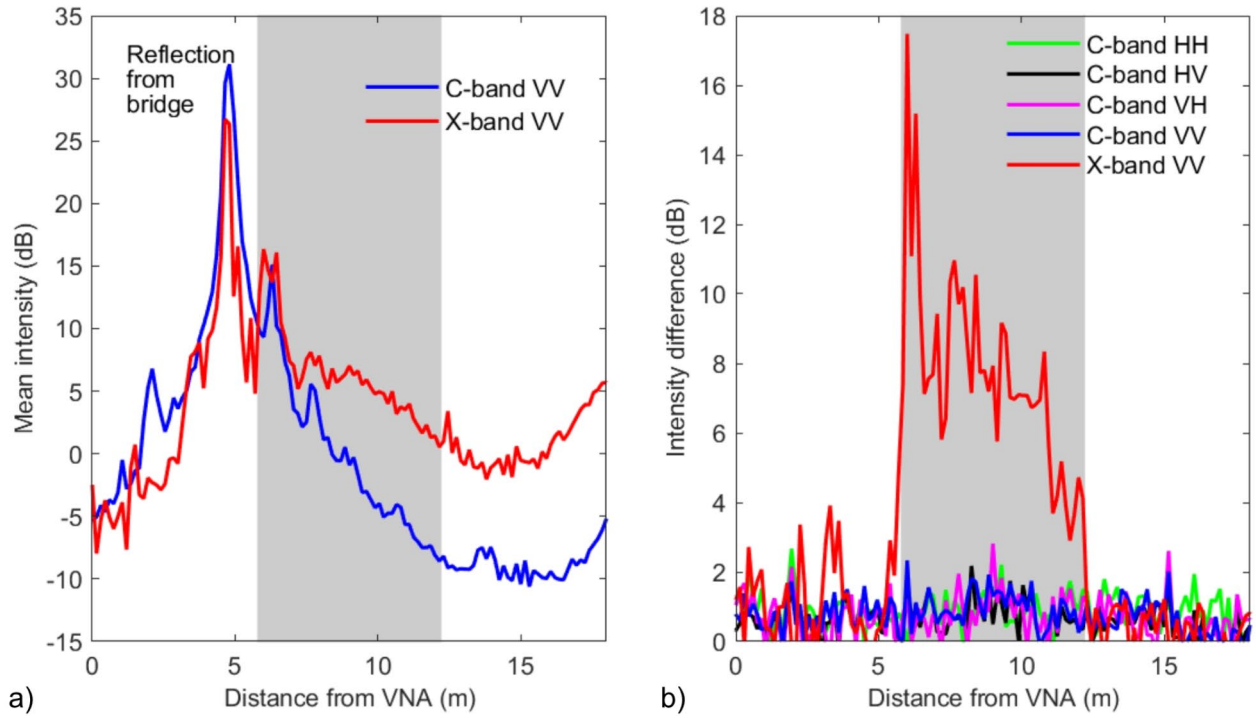


Fig. 3. (**a**) Intensity plot for the backscatter from plastic spheres at a concentration of 153 g/m^2 for C-band and X-band with different polarizations (HH, HV, VH, and VV) at Hs = 9 cm. The grey box shows the region of interest, where the signals reflect on the water surface. (**b**) intensity difference between plastic spheres and reference situation without plastics.

for mass concentrations higher than 20 g/m^2. This means that for higher wave heights more plastics are needed to reach the detectability threshold.

The best detection for C-band radar was found for fouled plastics. These are plastic sheets already fouled by organic matter attached to the plastic surface. The applied fouled plastics were collected in rivers and at riverbanks in the Netherlands. They consisted mainly of sheets and bags with a large surface area per plastic item. At C-band between 4 and 8 GHz, the fouled plastics were occasionally not detected, which could be related to the concentration in the field of view of the measurement instruments.

The length of the plastics items was varied for straws and for foam cylinders. The larger straws of 12 cm and 24 cm were better detectable than the smaller straws of 6 cm, which could be related to the wavelength of the X-band microwave which is about 3 cm. These wavelengths are longer for the lower frequency (L- to C-band) microwave signals (30 to 5 cm), which makes it harder to detect the plastics as the wavelength is larger than the plastics themselves. It must be noted that this behaviour was not observed for the foam cylinders where all tested cylinder lengths (5, 10 and 20 cm) met the detectability limit.

Regarding the shape of the objects, flatter, more film-like, shapes were seen to generate capillary waves from their interaction with the gravity waves we generated (Fig. 1b). These capillary waves are likely the more dominant form of scattering mechanism for these shapes. On the other hand, objects that are rounder, or larger items in general, will create a deeper imprint in the water surface. This could cause 'indentation' scattering (Fig. 1a - III) to be more prominent. These principles should be examined in more detail in future work.

The most observed plastics in nature (LDPE and PP) were best detectable using X-band microwaves. Polypropylene plastics were detected by C-band and higher and the fouled LDPE sheets were best detectable using X-band measurements. The only microplastics that were used in this test campaign were pellets with a size of 4 mm. These plastics were detectable by X-band microwaves and higher at a relatively high concentration of 20 g/m^2.

Concentration threshold for detection

Multiple tests were carried out using spheres with a diameter of 2 cm. At concentrations higher than 6.4 g/m^2 these plastic spheres could be detected at C-band with a bandwidth of 2 GHz and larger, giving a minimum concentration for the detection of these small plastic items. At a bandwidth of 1 GHz, the spheres and bottles were more difficult to detect. It has to be noted that the concentrations in our experiments are relatively high as compared to concentrations reported in ocean environments with (average) maximum mass concentrations in the ocean of 0.0025–0.1 g/m^2 [7,19]. However, due to inhomogeneity much higher concentrations (up to a factor 10^5) appear in marine litter windrows in oceans, where litter densities of 10 small items/m^2 or 1 large item

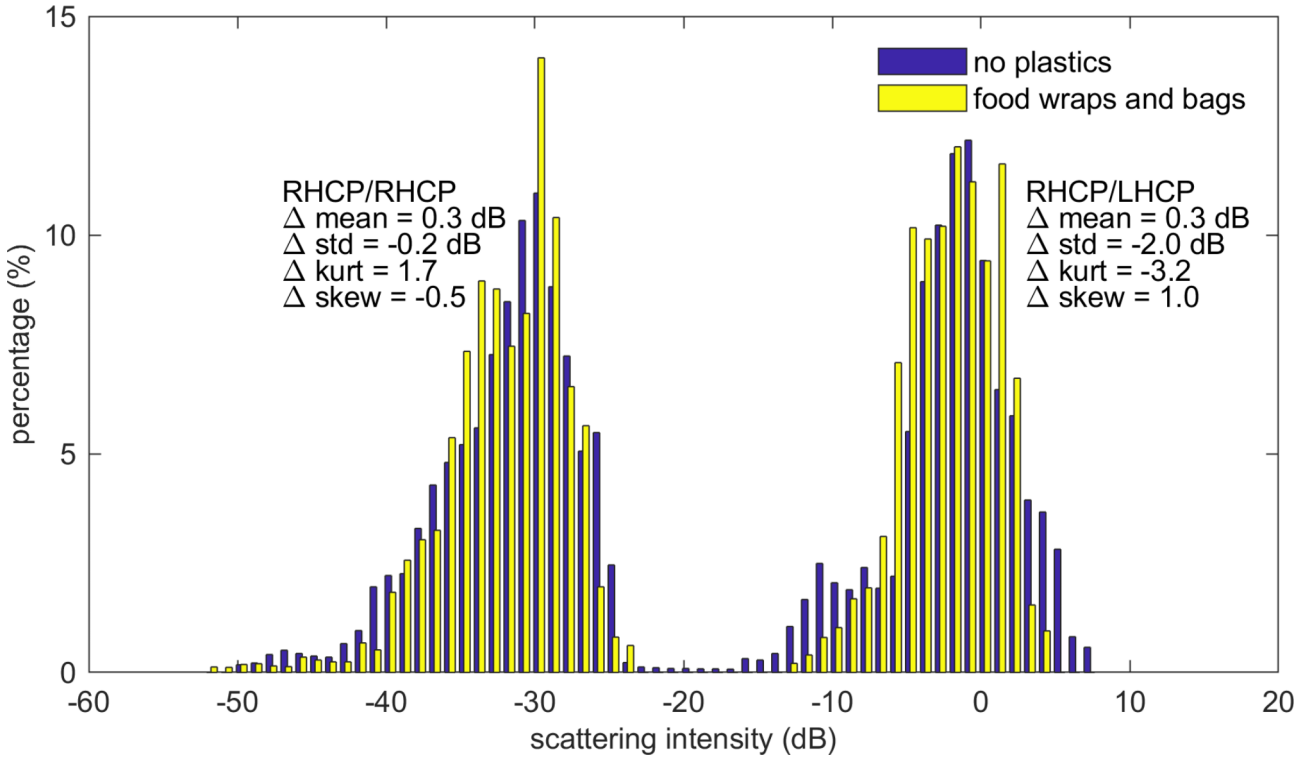


Fig. 4. Histograms of the reflectivity with and without plastics (flood wraps and bags) measured by GNSS-R (L1-band microwaves) at Hs = 9 cm. The signal is transmitted under an elevation angle of 30° with the vertical using right-hand central polarisation (RHCP) and is received both at right- (RHCP, left histogram) and left-hand central polarisation (LHCP, right histogram). The difference (Δ) in statistical parameters: mean, standard deviation, kurtosis and skewness are shown in the figure for the situation with plastics minus the situation without plastics.

per 10 m^2 are often exceeded[64]. Higher plastic litter concentrations can also be found upstream of hydraulic structures in waterways.

Concentration cannot be solely defined as a mass concentration in g/m^2, as the shape and number of objects has a significant impact on the scattering at microwave frequencies. In fact, the concentration of floating plastics can be determined based on mass, surface coverage and number of items. The detectability with X-band (10–12 GHz) at VV-polarisation is shown in Fig. 5 for all these three different concentration metrics.

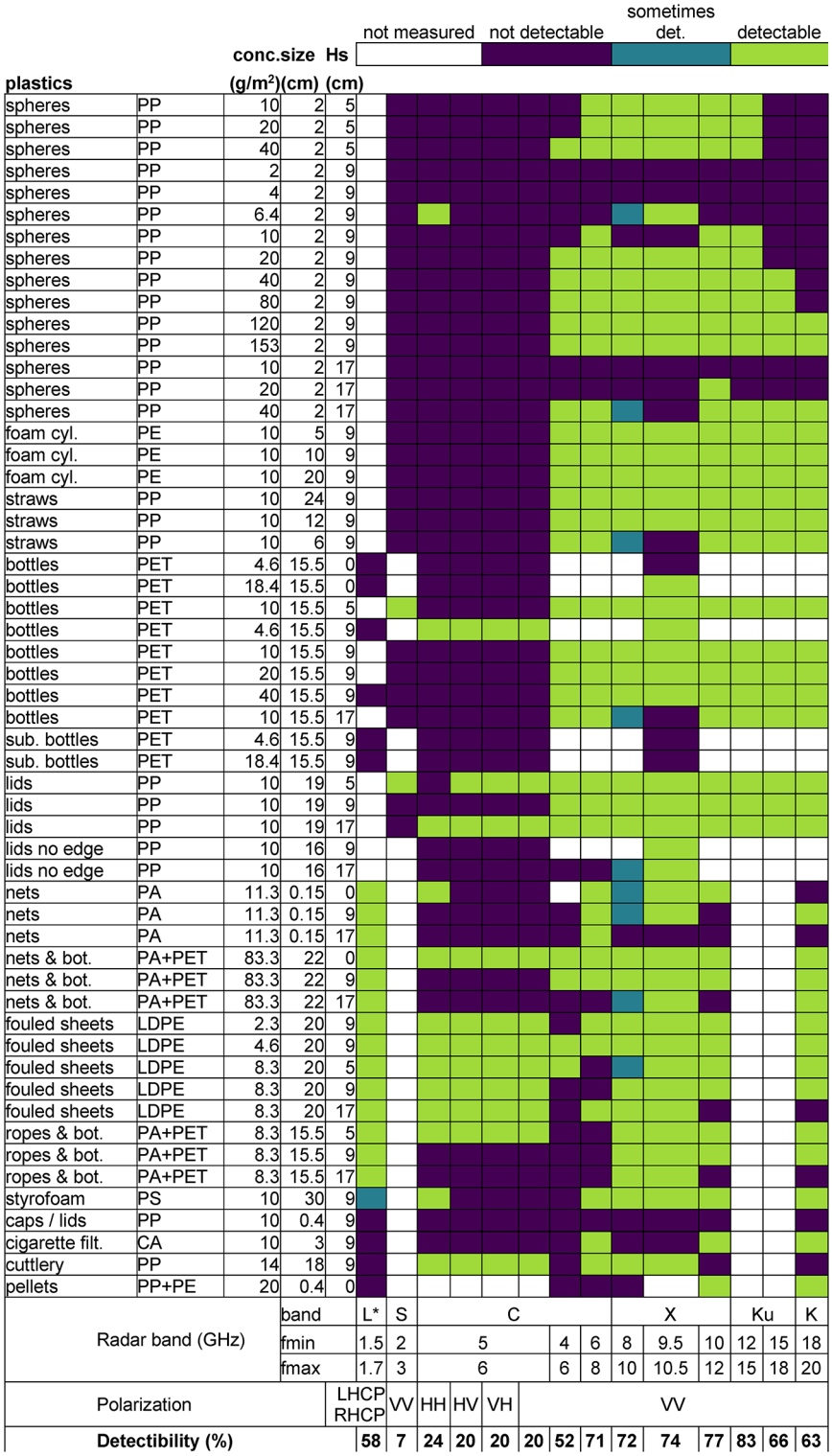
The concentrations are based on the concentrations of plastic supplied to the basin, which was monitored by a 4 K camera mounted at 8 m above the water surface. With this camera it was possible to determine the concentration of the spheres, the plastic bottles, and the straws. The other items could not be observed from this distance. Despite best efforts to control the concentration of objects in time and space, Eulerian currents, including cross flows, and air circulation within the basin moved and clumped together plastic items. For the measurement periods, mean concentrations were generally consistent with the desired concentrations except for a few high-wave-steepness cases when the plastic was swept downstream before the measurement had finished. A surface coverage correlation coefficient (r2) of 0.74 was found between the supplied concentration and the concentration based on camera detection (see Figure S9, Supplementary Material).

By investigating the maximum concentration when objects were non-detectable but present in the basin nonetheless, the threshold concentration for detection can be determined. In Table 3 the threshold concentration for detection is given per technique. From this table it is seen that the lowest concentration for detection is required for Ku-band with a frequency range between 12 and 15 GHz at VV polarization.

Optical sensor technologies

ASD optical measurements

With our lab setup, it turned out to be extremely difficult to detect floating plastics using the visible spectral range from 350 nm to 750 nm. For this reason, the spectral angles were calculated separately for the four spectral ranges to investigate if detection could be based on the NIR to SWIR2 ranges. The spectral angles for the NIR and SWIR1 were added and rotated by 90 degrees, providing a straightforward threshold to distinguish floating plastics by having negative values. This detection method was more challenging for bottles, where a threshold of 30 degrees was found. This method looks promising, but needs further evaluation[35,65] .



plastics		conc.size (g/m²)	Hs (cm)		L*	S	C			X		Ku		K
Radar band (GHz)		band			L*	S	C			X		Ku		K
		fmin			1.5	2	5		4	6	8	9.5	10	12	15	18
		fmax			1.7	3	6		6	8	10	10.5	12	15	18	20
Polarization				LHCP RHCP	VV	HH	HV	VH	VV							
Detectibility (%)				**58**	**7**	**24**	**20**	**20**	**20**	**52**	**71**	**72**	**74**	**77**	**83**	**66**	**63**
spheres	PP	10	2	5													
spheres	PP	20	2	5													
spheres	PP	40	2	5													
spheres	PP	2	2	9													
spheres	PP	4	2	9													
spheres	PP	6.4	2	9													
spheres	PP	10	2	9													
spheres	PP	20	2	9													
spheres	PP	40	2	9													
spheres	PP	80	2	9													
spheres	PP	120	2	9													
spheres	PP	153	2	9													
spheres	PP	10	2	17													
spheres	PP	20	2	17													
spheres	PP	40	2	17													
foam cyl.	PE	10	5	9													
foam cyl.	PE	10	10	9													
foam cyl.	PE	10	20	9													
straws	PP	10	24	9													
straws	PP	10	12	9													
straws	PP	10	6	9													
bottles	PET	4.6	15.5	0													
bottles	PET	18.4	15.5	0													
bottles	PET	10	15.5	5													
bottles	PET	4.6	15.5	9													
bottles	PET	10	15.5	9													
bottles	PET	20	15.5	9													
bottles	PET	40	15.5	9													
bottles	PET	10	15.5	17													
sub. bottles	PET	4.6	15.5	9													
sub. bottles	PET	18.4	15.5	9													
lids	PP	10	19	5													
lids	PP	10	19	9													
lids	PP	10	19	17													
lids no edge	PP	10	16	9													
lids no edge	PP	10	16	17													
nets	PA	11.3	0.15	0													
nets	PA	11.3	0.15	9													
nets	PA	11.3	0.15	17													
nets & bot.	PA+PET	83.3	22	0													
nets & bot.	PA+PET	83.3	22	9													
nets & bot.	PA+PET	83.3	22	17													
fouled sheets	LDPE	2.3	20	9													
fouled sheets	LDPE	4.6	20	9													
fouled sheets	LDPE	8.3	20	5													
fouled sheets	LDPE	8.3	20	9													
fouled sheets	LDPE	8.3	20	17													
ropes & bot.	PA+PET	8.3	15.5	5													
ropes & bot.	PA+PET	8.3	15.5	9													
ropes & bot.	PA+PET	8.3	15.5	17													
styrofoam	PS	10	30	9													
caps / lids	PP	10	0.4	9													
cigarette filt.	CA	10	3	9													
cuttlery	PP	14	18	9													
pellets	PP+PE	20	0.4	0													

Table 2. Detectability of the plastics using microwave technologies. The wave conditions, the type of plastic, the concentration and the size of the plastic items is varied (see supplementary material). In table 1, an overview is presented of the different microwave technologies. The C-band (4–6 GHz and 6–8 GHz) and X-band (8–10 GHz) with VV polarization was measured by two setups with different look-up angles. When only one device detected the plastic, it is referred to as "sometimes detectable". * the detectability for L band is based on statistical analysis (see 3.1.3), while the detectability for S- to K-band is based on the level of backscattering.

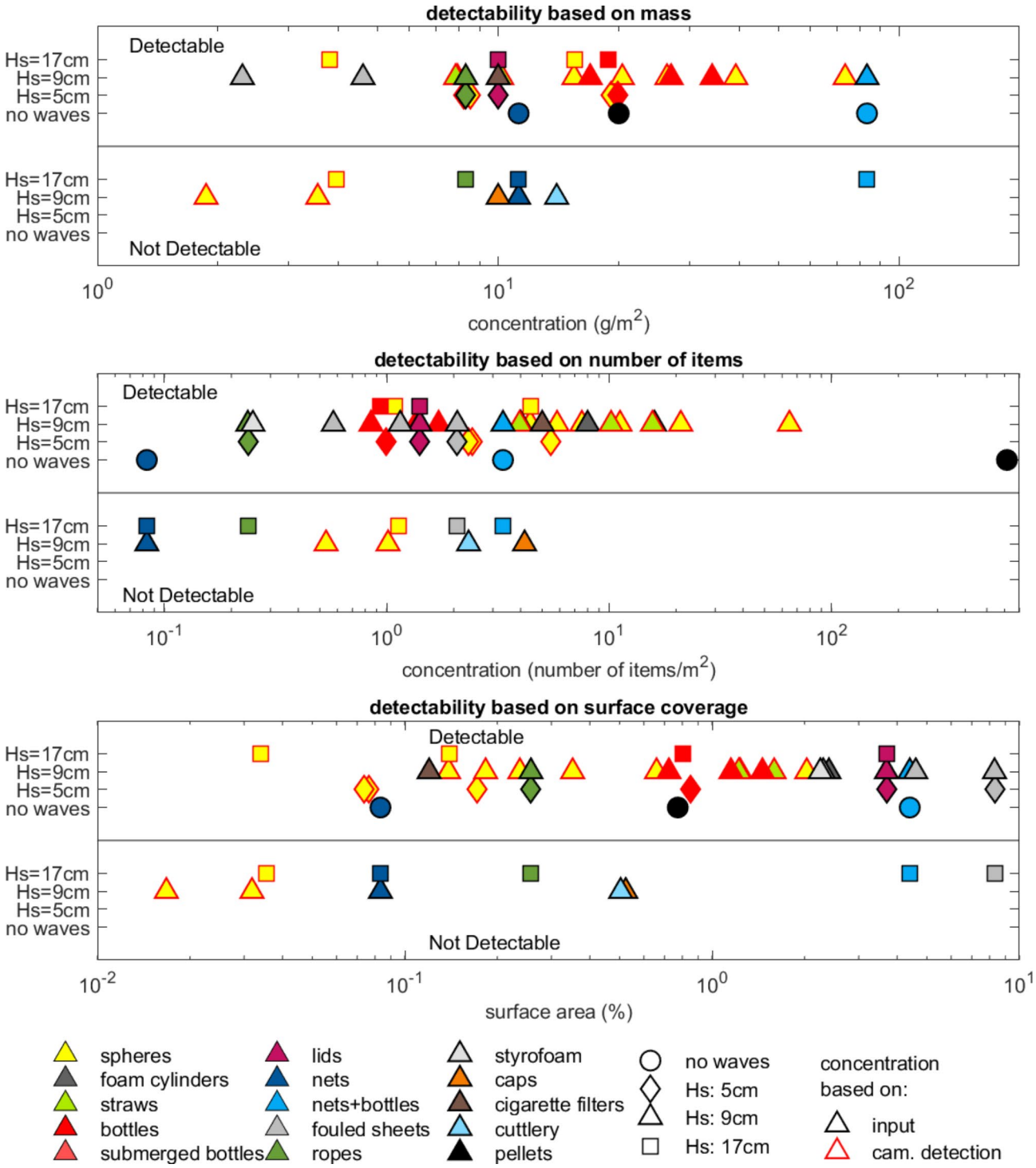


Fig. 5. Detectability for X-band (10–12 GHz) at VV polarisation for three different plastic concentration metrics. The plastic concentration is shown as concentration based on mass (top), concentration based on number of items (middle) and concentration based on surface coverage (bottom). Markers with black outline show concentrations that are based on the input concentration and markers with red outlines show concentrations that are based on camera measurements (for spheres, bottles and straws only).

Polarimetric measurements

Initial results from the GroundSPEX and the RGB polarization camera showed a moderate degree of linear polarization (DoLP) between 0.05 and 0.15 of light reflected by several types of plastics (Fig. 6). Comparing the red-green-blue (RGB) photograph and the green-band polarization of a transparent lids and floating bottle image suggests four primary mechanisms for polarization. First, direct specular reflection off plastic objects,

Radar band	f_{min}-f_{max} (GHz)	Supplied conc. / Polarization	Mass conc. (g/m2) 1-226	Number conc. (items/m2) 0.05–615	Surface cov. (%) 1e-2 – 8.3%
L* (GNSS-R)	1.5–1.7	LHCP&RHCP	27	615	1.2%
S	2–3	VV	226	65	3.7%
C	5–6	HH	226	65	4.4%
		HV	226	65	4.4%
		VH	226	65	4.4%
		VV	226	65	4.4%
	4–6		83	615	8.3%
	6–8		83	615	8.3%
X	8–10		20	615	0.8%
	9.5–10.5		20	16	1.2%
	10–12		83	4	8.3%
KU	12–15		4	1	4e-2%
	15–18		20	6	0.2%
K	18–20		39	11	8.3%

Table 3. Plastic detection thresholds for three different concentration metrics: mass concentration, number concentration and surface coverage. * the detectability for L band is based on statistical analysis (see 3.1.3), while the detectability for S- to K-band is based on the level of backscattering.

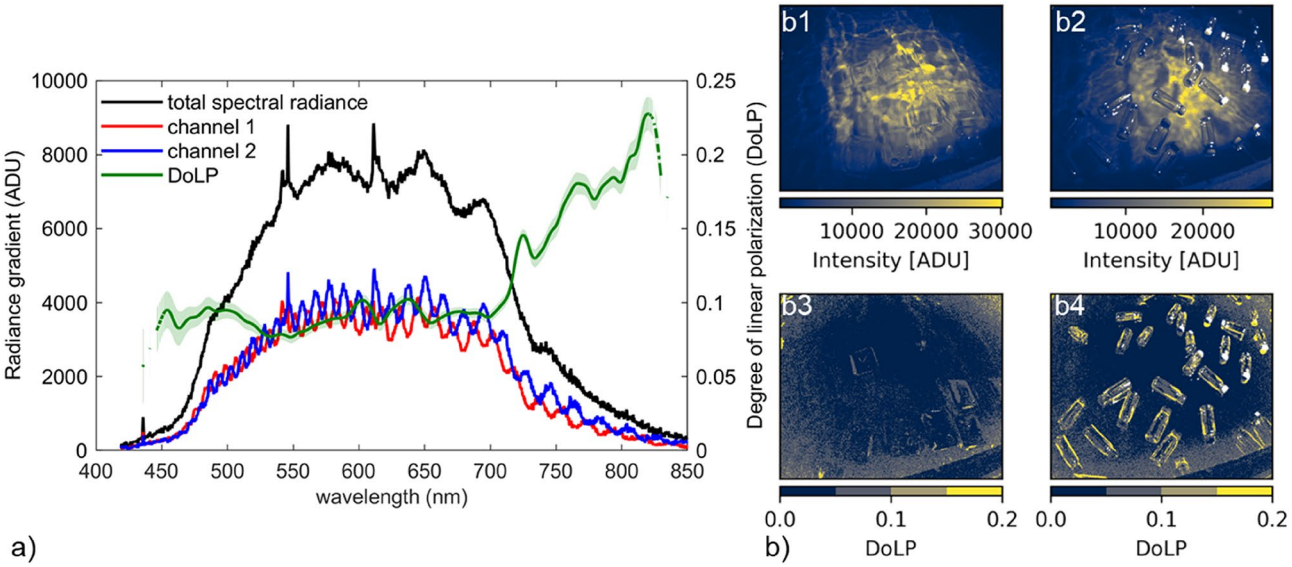


Fig. 6. (**a**) GroundSPEX radiance and degree of linear polarization from floating bottles with Hs = 17 cm. The raw data from the two spectroradiometer channels (red and blue lines) highlight the SPEX sinusoidal modulation. The black line represents the total spectral radiance and the green line represents the degree of linear polarization retrieved from the data. (**b**) BlackFly observations in green band for transparent lids (b1, b3 – not detectable) and bottles (b2, b4 - detectable) for radiance (b1, b2) and degree of linear polarisation (b3, b4).

such as bottles, produced a very bright and angle-dependent signal, which can be identified in the DoLP image (Fig. 6b). Second, indentations (Fig. 1) and small waves formed on top of objects, such as sheets and foams, producing weak polarization signals. Third, images containing specular reflection of plastic objects, particularly large and opaque ones, on the water surface were highly polarized but typically dim. Fourth, light scattered off dark objects, such as tarps and plastic bags, was moderately polarized but also dim, reminiscent of the single-scattering Umov effect[66]. The polarization signals were found to be spectrally flat, suggesting that hyperspectral measurements may not provide an advantage over RGB imagery.

Overview optical sensor technologies. Table 4 shows the detectability by the optical instruments. The detection of the plastics is based on radiance from the ASD and on polarization from GroundSPEX and the RGB

plastics		size (cm)	Hs (cm)			
spheres	PP	2	9			
foam cyl.	PE	5	9			
foam cyl.	PE	10	9			
foam cyl.	PE	20	9			
foam cyl.	PE	raft	5			
foam cyl.	PE	raft	9			
bubble wrap		30				
straws	PP	24	9			
straws	PP	6	9			
straws	PP	12	17			
straws	PP	raft	0			
straws	PP	raft	5			
straws	PP	raft	9			
bottles	PET	15.5	0			
bottles	PET	15.5	5			
bottles	PET	15.5	9			
bottles	PET	15.5	17			
lids	PP	19	5			
lids	PP	19	9			
lids	PP	19	17			
lids no edge	PP	16	9			
lids no edge	PP	16	17			
nets	PA	0.15	5			
nets	PA	0.15	9			
nets	PA	0.15	17			
org. sheets	LDPE	20	9			
styrofoam	PS	30	9			
	Wavelength (nm)		λmin	470	400	400
			λmax	870	900	700
	Optical instrument			** ASD fieldspec	GroundSPEX	BlackFly pol. camera
	Detectibility (%)			**88**	**43**	**46**

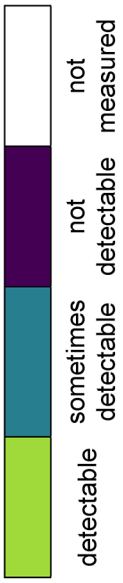


Table 4. Detectability of the plastics using optical technologies under various wave conditions. The type of plastic, the concentration and the size of the plastic items is varied. In Table 1, an overview is presented of the different microwave technologies. **The detectability for the ASD is based on a limited number of 4 measurements only.

polarisation camera. A moderate degree of linear polarization ($0.05 \leq \text{DoLP} \leq 0.20$) of reflected light was found for several types of plastic litter, particularly dark objects, which are difficult to detect with existing non-polarized techniques. Transparent lids were difficult to detect, where a difference was seen for lids with edges that were slightly above the water surface and lids without edges that follow the water surface. For the foam cylinders and the straws, it did not make a difference if the plastics were distributed normally or if they were clustered together in so-called "rafts" (see supplementary material). For the reflected signals to the RGB polarisation camera, it was observed that for some plastics, such as straws, the detectability was based on the rotation angle of the plastics which lead to glints that could be detected. Table 4 shows that optical polarization measurements are a promising method for detecting plastics, encouraging further research and application.

Discussion

This extensive laboratory study of the detection of floating plastic litter highlights the capabilities of different remote sensing techniques in the presence of scaled ocean waves. Plastics were detected using different microwave and optical instruments. For microwave instruments, the best way to detect plastics from the scattering signal was by using frequency bands in the range of X and Ku-band at VV polarization for number concentrations higher

than 1 item/m^2 or mass concentrations of 1–10 g/m^2. This could be sufficient to identify marine litter windrows where higher concentrations of plastics are observed[64]. The proposed plastic detection criterion is based only on the excess (above a threshold) power scattered by the sea surface. In a scenario where the properties of the plastic litter are unknown, this approach only allows the identification of the presence of floating targets, not of any of its physical properties. Unsupervised identification of those properties would require complementary techniques, such as machine learning. In our experiments, it was observed that plastic detection for microwaves depends on plastic type, plastic length, and water-wave height in the field of view.

A key finding from the microwave results is that as wave height increases, detection of small plastic targets decreases. This can be found in the literature with satellite or ground-based observations[42]. It has previously been observed that VV polarization in Sentinel-1 data (C-band) can be used for monitoring and detecting plastic targets[38,55]. Detection of plastics using X-band microwaves has been studied less. The results from this measurement campaign give insight in the capabilities of detection for less studied bands. At L-band, the changes in the forward-scattered signal power are marginal, and barely detectable even with a 0.02 dB sensitivity. For this reason, an analysis on the statistical descriptors has been used. GNSS-reflectometry can detect marine plastic litter. However, extrapolation of results to airborne and spaceborne cases is not straightforward and requires careful consideration.

This article focuses only on floating plastics that were detected by remote sensing technologies in a laboratory environment using freshwater conditions without wind that might influence the plastic movement. Applying these findings of these idealized measurements to field conditions using airborne or satellite measurements will require several challenges to overcome. Although the tests carried out in the Deltares test facility provide a good indication of the possibility to detect plastics using microwave remote sensing technologies, some caution and additional analysis are required to extrapolate the results to airborne and spaceborne applications.

Crucially, the high-frequency (i.e., capillary-wave-dominated) part of the surface wave spectrum in our experiments is not necessarily representative of the real ocean. We recommend experiments in which the capillary-wave-dominated part of the surface wave spectrum is carefully controlled. In our experiments we ensure a similar ratio between experiment and ocean conditions for litter size and electromagnetic wavelength and between surface water wavelength and water wave height on the other hand to be representative of the field, as we believe these are the two most important non-dimensional numbers. However, relative to the electromagnetic wavelength and to litter size, our surface water wavelength is much too small. This can only be remedied by conducting experiments in the field or only partly in even larger experimental facilities, of which there are only very few in the world.

The following aspects need to be analysed before translating the study to an airborne/spaceborne setup. The applied formulation and metrics present no limitations if the antenna footprint scales to much larger areas, as long as litter concentration remains uniform over the enlarged footprint and compatible signal power level are transmitted. Wind will add differences in the scattered signal statistics, by producing areas with varying capillary wave intensity in the area of interest. In the experiments we had control of the reference case with waves but without plastic, while this would not be the case in the real world, where the reference has to be extracted locally in terms of areas deemed free from plastic but having similar wave conditions. Finally, moderately wide frequency band were used in our measurement campaign without considering regulatory constraints, to reveal all the physics involved in the scattering process. However, when transmitting from space, the bandwidth used, must conform to regulated bands, which mostly involve smaller bandwidths. The corresponding impact needs to be evaluated. In our measurements, we have not been analysing atmospheric effects and Doppler shifts, because there is knowledge in the literature to factor these out by post-processing[67–69].

Our optical experiments showed that for unpolarized measurements, the visible spectral range offers limited detection capability of floating plastics. This differs from published successful detection of floating plastic in laboratories or airplanes[34,35,46,70] and this is likely due to the effects of fluorescent light during the experiment. The combination of multiple reflections from the sides of the tank (walls and bottom) and the specular reflection from the fluorescent light on the water surface all contributed to masking the detection capability for the visible part of the solar spectrum. Nonetheless, similar situations are plausible in natural conditions, for example for scenes affected by sun glint or optically shallow waters. The results are obtained from lab-controlled conditions with small footprints (1.6 to 14 cm in diameter). Comparing this to the current high-resolution sensors, e.g. Sentinel-2 MSI that has a nominal pixel area of 100 m^2, and adding the effects of atmospheric path radiance indicates the challenges for upscaling. The magnitude of detectable reflectance from plastics has been shown to be impacted by the inherent pixel coverage and sensitivity of instrument used to conduct measurements[38,46,71,]. We found that spectropolarimetry can play a role in identifying dark floating plastic objects, but it is unlikely that current optical missions, which do not consider polarization, and current and future spectropolarimetric sensors on satellites, will be able to distinguish the polarized reflectance of floating plastic litter from other constituents, bubbles and whitecaps, specular reflections, and atmospheric signals[59,72]. The linear polarization experiments in the test campaign represent a situation where the sensor field of view is entirely filled with floating plastic litter, which is not realistic for satellite sensors. Instead, these conditions are more similar to UAV- and ship-mounted setups, which can resolve individual objects and may well benefit from using polarization cameras to detect and track them, particularly for colourless and dark objects.

The effects of conglomeration and dispersal by currents, the fading nature of weathering and degrading floating plastics and the effects of biofouling all impact the detection of plastics. For optics, comprehensive overview of plastic versus other floating materials (Sargassum, wood etc.) are provided[37,44,73], while this requires additional investigation for microwaves. In the microwave ranges, Sargassum will appear as a bright mat on the surface of water, as it increases the roughness and therefore backscattering[50]. Oil dampens waves and reduces the surface roughness, so this appears darker within the images[51]. And plastic appears as a mix of both, either

through a large accumulation of macroplastics increasing the backscattering or via microbial surfactants on plastic.

Data availability

The measurement data generated in this study have been deposited in the Zenodo database and can be accessed via this link: https://doi.org/10.5281/zenodo.10458751.

Received: 1 March 2024; Accepted: 25 September 2024
Published online: 29 October 2024

References

1. Waters, C. N. et al. The Anthropocene is functionally and stratigraphically distinct from the Holocene. *Science*. **351**, 2622. https://doi.org/10.1126/science.aad2622 (2016).
2. Ostle, C. et al. The rise in ocean plastics evidenced from a 60-year time series. *Nat. Commun.***10**, 1622. https://doi.org/10.1038/s41467-019-09506-1 (2019).
3. MacLeod, M. et al. The global threat from plastic pollution. *Sci. Vol.* **373**, 61–65. https://doi.org/10.1126/science.abg5433 (2021).
4. Thushari, G. G. N. & Senevirathna, J. D. M. Plastic pollution in the marine environment. *Heliyon*. **6**, 8. https://doi.org/10.1016/j.heliyon.2020.e04709 (2020). e04709.
5. Jambeck, J. R. et al. Plastic waste inputs from land into the ocean. *Science*. **347**, 768–771. https://doi.org/10.1126/science.1260352 (2015).
6. Van Sebille, E. et al. The physical oceanography of the transport of floating marine debris. *Environ. Res. Lett.***15**, 023003. https://doi.org/10.1088/1748-9326/ab6d7d (2020).
7. Lebreton, L. et al. Evidence that the great pacific garbage patch is rapidly accumulating plastics. *Sci. Rep.***8**, 4666. https://doi.org/10.1038/s41598-018-22939-w (2018).
8. Andrady, A. L. Persistence of plastic litter in the oceans. Ch.3. in M. Bergmann, L. Gutow & M. Klages (Eds.), *Marine Anthropogenic Litter*, 57–72 (2015). https://doi.org/10.1007/978-3-319-16510-3
9. Lusher, A. L., McHugh, M. & Thompson, R. C. Occurrence of mirocplastics in the gastrotenstial tract of pelagic and demersal fish from the English Channel. *Mar. Pollut Bull.***67**, 94–99. https://doi.org/10.1016/j.marpolbul.2012.11.028 (2013).
10. Foekema, E. M. et al. Plastic in North sea fish. *Environ. Sci. Technol.***47**, 8818–8824. https://doi.org/10.1021/es400931b (2013).
11. Besseling, E. et al. Microplastic in a macro filter feeder: Humpback whale *Megaptera novaeangliae*. *Mar. Pollut. Bull.* **95**, 248–252. https://doi.org/10.1016/j.marpolbul.2015.04.007 (2015).
12. Bergman, M., Gutow, L. & Klages, M. *Marine Anthropogenic Litter*, https://doi.org/10.1007/978-3-319-16510-3 (2015).
13. Tekman, M. B. et al. Litterbase – Online portal for marine litter & microplastics and their implications for marine life, Alfred Wegener Institute Helmholtz Centre for Polar and Marine Research. http://litterbase.org/ (last accessed 8 October 2024).
14. Reisser, J. et al. The the vertical distribution of buoyant plastics at sea: An observational study in the North Atlantic Gyre. *Biogeosci*. **12**, 1249–1256. https://doi.org/10.5194/bg-12-1249-2015 (2015).
15. Valero, D. et al. The key role of surface tension in the transport and quantification of plastic pollution in rivers. *Water Res.***226**, 119078. https://doi.org/10.1016/j.watres.2022.119078
16. Chen, X. et al. Sinking of floating plastic debris caused by biofilm development in a freshwater lake. *Chomosphere*. **222**, 856–864. https://doi.org/10.1016/j.chemosphere.2019.02.015 (2019).
17. Pabortsava, K. & Lampitt, R. S. High concentrations of plastic hidden beneath the surface of the Atlantic Ocean. *Nat. Commun.***11**, 4073. https://doi.org/10.1038/s41467-020-17932-9 (2020).
18. Kooi, M. et al. The effect of particle properties on the depth profile of buoyant plastics in the ocean. *Sci. Rep.* **6**, 33882. https://doi.org/10.1038/srep33882 (2016).
19. Cózar, A. et al. Plastic debris in the open ocean. *PNAS*. **111** (28), 10239–10244. https://doi.org/10.1073/pnas.1314705111 (2014).
20. Zhang, Y. et al. Plastic waste discharge to the global ocean constrained by seawater observations. *Nat. Commun.***14**, 1372. https://doi.org/10.1038/s41467-023-37108-5 (2023).
21. Van Sebille, E. et al. Origin, dynamics and evolution of ocean garbage patches from observed surface drifters. *Environ. Res. Lett.* **7** 044040. (2012). https://doi.org/10.1088/1748-9326/7/4/044040.
22. Galgani, F., Hanke, G. & Maes, T. Global distribution, composition and abundance of marine litter, Ch.2 in Bergmann M., Gutow L., Klages M. (eds) 29–56 (2015). https://doi.org/10.1007/978-3-319-16510-3_2
23. Van Sebille, E. et al. A global inventory of small floating plastic debris. *Environ. Res. Lett.***10**, 124006. https://doi.org/10.1088/1748-9326/10/12/124006 (2015).
24. Eriksen, M. et al. Plastic Pollution in the World's oceans: More than 5 trillion plastic pieces weighing over 250,000 tons afloat at sea. *PLoS ONE*. **9** (12), e111913. https://doi.org/10.1371/journal.pone.0111913 (2015).
25. Lebreton, L. et al. A global mass budget for positively buoyant macroplastic debris in the ocean. *Sci. Rep.* **9**, 12922. https://doi.org/10.1038/s41598-019-49413-5 (2019).
26. Wilcox, C. et al. Abundance of floating plastic particles is increasing in the Western North Atlantic Ocean. *Environ. Sci. Technol.***54** (2), 790–796. https://doi.org/10.1021/acs.est.9b04812 (2019).
27. Geyer, R. et al. Production, use, and fate of all plastics ever made. *Sci. Adv.***3** (7), e1700782. https://doi.org/10.1126/sciadv.170078 (2017).
28. Kaandorp, M. L. A. et al. Global mass of buoyant marine plastics dominated by large long-lived debris. *Nat. Geosci.***16**, 689–694. https://doi.org/10.1038/s41561-023-01216-0 (2023).
29. Addamo, A. M., Laroche, P. & Hanke, G. Top marine beach litter items in Europe – a review and synthesis based on beach litter data, European Commission, EUR 29249 EN, JRC technical reports, JRC108181, (2017). https://doi.org/10.2760/496717
30. Erni-Cassola, G. et al. Distribution of plastic polymer types in the marine environment; a meta-analysis. *J. Haz. Mat.* **369**, 691–698. https://doi.org/10.1016/j.jhazmat.2019.02.067 (2019).
31. Schwarz, A. E. et al. Sources, transport, and accumulation of different types of plastic litter in aquatic environments: A review study. *Mar. Pollut Bull.***143**, 92–100. https://doi.org/10.1016/j.marpolbul.2019.04.029 (2019).
32. Lacroix, C. et al. Abundance, Composition and Trends of Beach Litter – common indicator assessment. In: OSPAR, The 2023 Quality Status Report for the North-East Atlantic. OSPAR Commission, London. https://oap.ospar.org/en/ospar-assessments/quality-status-reports/qsr-2023/indicator-assessments/beach-litter (2023).
33. GESAMP & UNEP/UNDP/ISA Joint Group of Experts on the Scientific Aspects of Marine Environmental Protection) International Maritime Organization - London, UK, 130 p., Guidelines or the monitoring and assessment of plastic litter and microplastics in the ocean. (IMO/FAO/UNESCO-IOC/UNIDO/WMO/IAEA/UN/ (2019). http://www.gesamp.org/publications/guidelines-for-the-monitoring-and-assessment-of-plastic-litter-in-the-ocean
34. Garaba, S. P. et al. Hyperspectral longwave infrared reflectance spectra of naturally dried algae, anthropogenic plastics, sand and shells. *Earth Syst Sci. Data*. **12** (4), 2665–2678. https://doi.org/10.5194/essd-12-2665-2020 (2020).

35. Garaba, S. P. et al. Sensing ocean plastics with an airborne hyperspectral shortwave infrared imager. *Environ. Sci. Technol.***52** (20), 11699–11707. https://doi.org/10.1021/acs.est.8b02855 (2018).
36. Goddijn-Murphy et al. Using a UAV thermal infrared camera for monitoring floating marine plastic litter. *Remote Sens.***14** (13), 3179. https://doi.org/10.3390/rs14133179 (2022).
37. Hu, C. Remote detection of marine debris using satellite observations in the visible and near infrared spectral range: Challenges and potentials. *Remote Sens. Environ.***259**, 112414. https://doi.org/10.1016/j.rse.2021.112414 (2021).
38. Topouzelis, K. et al. Detection of floating plastics from satellite and unmanned aerial systems (Plastic Litter Project 2018). *Int. J. Appl. Earth Obs Geoinf.***79**, 175–183. https://doi.org/10.1016/j.jag.2019.03.011 (2019).
39. Papageorgiou, D. et al. Sentinel-2 detection of floating marine litter targets with partial spectral unmixing and spectral comparison with other floating materials (Plastic Litter Project 2021). *Remote Sens.***14** (23), 5997. https://doi.org/10.3390/rs14235997 (2022).
40. Park, Y. J. et al. Detecting the great pacific garbage patch floating plastic litter using WorldView-3 satellite imagery. *Opt. Express*. **29** (22), 35288–35298. https://doi.org/10.1364/OE.440380 (2021).
41. GIZ, Advances in remote sensing of plastic waste, Deutsche Gesellschaft für Internationale Zusammenarbeit (GIZ) GmbH, edited by: Giang, P., and Ortwig, N., Eschborn, Germany, 88 pp. (2023). https://www.giz.de/en/downloads/giz-2023-en-advances-in-remote-sensing-of-plastic-waste.pdf
42. Martínez-Vicente, V. et al. Measuring marine plastic debris from space: Initial assessment of observation requirements. *Remote Sens.* **11** (20), 2443. https://doi.org/10.3390/rs11202443 (2019).
43. Maximenko, N. et al. Toward the integrated marine debris observing system. *Front. Mar. Sci.* **6**, 447. https://doi.org/10.3389/fmars.2019.00447 (2019).
44. Dierssen, H. M., Garaba, S. P. & Bright Oceans Spectral differentiation of whitecaps, sea ice, plastics, and other flotsam, in (eds Vlahos, P. & Monahan, E. C.) *Recent Advances in the Study of Oceanic Whitecaps: Twixt Wind and Waves*: Cham, Springer International Publishing, 197–208 https://doi.org/10.1007/978-3-030-36371-0_13 (2020).
45. Goddijn-Murphy, L. & Dufaur, J. Proof of concept for a model of light reflectance of plastics floating on natural waters. *Mar. Pollut Bull.***135**, 1145–1157. https://doi.org/10.1016/j.marpolbul.2018.08.044 (2018).
46. Garaba, S. P. et al. Concentration, anisotropic and apparent colour effects on optical reflectance properties of virgin and ocean-harvested plastics. *J. Haz Mat.***406**, 124290. https://doi.org/10.1016/j.jhazmat.2020.124290 (2021).
47. Salgado-Hernanz, P. M. et al. Assessment of Marine Litter through Remote sensing: Recent approaches and future goals. *Mar. Pollut Bull.***168**, 112347. https://doi.org/10.1016/j.marpolbul.2021.112347 (2021).
48. Davaasuren et al. Detecting microplastic pollution in world oceans using SAR remote sensing, IGARSS (2018). https://doi.org/10.1109/IGARSS.2018.8517281
49. Simpson, M. et al. Monitoring surfactants pollution potentially related to plastics in the world gyres using radar remote sensing, IGARSS (2021). https://doi.org/10.1109/IGARSS47720.2021.9553406.
50. Qi, L. et al. On the capacity of Sentinel-1 synthetic aperture radar in detecting floating macroalgae and other floating matters. *Remote Sens. Environ.***280**, 113188. https://doi.org/10.1016/j.rse.2022.113188 (2022).
51. Alpers, W. et al. Oils and surfactants, in Synthetic Aperture Radar Marine User's Manudited by C. R. Jackson and J. R. Apel, 263–275, U.S. Dep. of Commer., Washington, D. C. (2004). https://www.sarusersmanual.com/ManualPDF/NOAASARManual_CH11_pg263-276.pdf
52. Simpson, M. et al. Monitoring of plastic Islands in river environment using sentinel-1 SAR data. *Remote Sens.***14**, 4473. https://doi.org/10.3390/rs14184473 (2022).
53. Fuentes Reyes, M. et al. SAR-to-optical image translation based on conditional generative adversarial networks—optimization, opportunities and limits. *Remote Sens***11**(17), 2067. https://doi.org/10.3390/rs11172067 (2019).
54. Felicio, J. et al. Feasibility of radar-based detection of floating macroplastics at microwave frequencies. *IEEE Trans. Antennas Propag.* , **72**(3), 2766–2779. https://doi.org/10.1109/TAP.2023.3347031 (2024).
55. Simpson, M. et al. Investigating the backscatter of marine plastic litter using a C- and X-band ground radar, during a measurement campaign in Deltares. *Remote Sens.***15**, 1654. https://doi.org/10.3390/rs15061654 (2023).
56. Gonga, A. et al. Observations of Marine Plastic Litter in a Water Flume: An experimental study. *Remote Sens.* **15**, 637. https://doi.org/10.3390/rs15030637 (2023).
57. Burggraaff, O. et al. Standardized spectral and radiometric calibration of consumer cameras. *Opt. Express.* **27** (14), 19075–19101. https://doi.org/10.1364/OE.27.019075 (2019).
58. Van Harten et al. Atmospheric aerosol characterization with a ground-based SPEX spectropolarimetric instrument. *Atmos. Meas. Tech.***7**, 4341–4351. https://doi.org/10.5194/amt-7-4341-2014 (2014).
59. Burggraaff, O. Accessible remote sensing of water, PhD dissertation, Universiteit Leiden, ISBN 978-94-6421-952-4, (2022). https://hdl.handle.net/1887/3497379
60. Sun, Y. et al. Effects of microplastics and surfactants on surface roughness of water waves. *Sci. Rep.* **13**, 1978. https://doi.org/10.1038/s41598-023-29088-9 (2023).
61. Stokes, G. G. On the theory of oscillatory waves. *Trans. Camb. Philos. Soc.***8**, 441–455 (1847).
62. Van den Bremer, T. & Breivik, Ø. Stokes drift. *Phil. Trans. R Soc. A.* **376**, 20170104. https://doi.org/10.1098/rsta.2017.0104 (2017).
63. Eeltink, D. et al. Stochastic particle transport by deep-water irregular breaking waves. *J. Fluid Mech.***971**https://doi.org/10.1017/jfm.2023.671 (2023).
64. Cozar, A. et al. Marine litter windrows: A strategic target to understand and manage the ocean plastic pollution. *Front. Mar. Sci.***8**, 571796. https://doi.org/10.3389/fmars.2021.571796 (2021).
65. Kruse, F. A. et al. The spectral image processing system (SIPS) interactive visualization and analysis of imaging spectrometer data. *Remote Sens. Environ.***44**:145–163, https://doi.org/10.1016/0034-4257(93)90013-N (1993).
66. Umov, N. Chromatische Depolarisation Durch Lichtzerstreuung. *Phys. Z.***6** (20), 674–676 (1905).
67. Franceschetti, G. et al. *Synthetic Aperture Radar Processing*, 1st Edition, CRC Press, ISBN 9780849378997 (1999).
68. Carreno-Luengo, H. & Camps, A. Empirical results of a surface-level GNSS-R experiment in a Wave Channel. *Remote Sens.***7** (6), 7471–7493. https://doi.org/10.3390/rs70607471 (2015).
69. Asgarimehr, M. et al. Remote sensing of precipitation using reflected GNSS signals: Response analysis of polarimetric observations. *IEEE. Trans. Geosci. and Remote Sens.* **60**, 5800412.https://doi.org/10.1109/TGRS.2021.3062492 (2021).
70. Moshtaghi et al. Spectral reflectance of marine macroplastics in the VNIR and SWIR measured in a controlled environment. *Sci. Rep.***11**, 5436. https://doi.org/10.1038/s41598-021-84867-6 (2021).
71. Garaba, S. P. & Park, Y. J. Riverine litter monitoring from multispectral fine pixel satellite images. *Environ. Adv.***15**, 100451. https://doi.org/10.1016/j.envadv.2023.100451 (2024).
72. Ottaviani, M. et al. Remote sensing of the ocean surface refractive index via short-wave infrared polarimetry. *Remote Sens. Environ.***221**, 14–23. https://doi.org/10.1016/j.rse.2018.10.016 (2019).
73. De Vries, R. et al. Hyperspectral reflectance of pristine, ocean weathered and biofouled plastics from a dry to wet and submerged state. *Earth Syst. Sci. Data*. **15**, 5575–5596. https://doi.org/10.5194/essd-15-5575-2023 (2023).

Acknowledgements

This work has been performed as part of the OSIP and Discovery programmes of the European Space Agency (ESA). We thank P. Corradi, the Technical Officer and Coordinator of the ESA Discovery Campaign on Remote

Sensing of Plastic Marine Litter for this cooperation during this project. Multiple authors were funded by these programmes from different grants. UPC activities were also partially sponsored by project "GENESIS: GNSS Environmental and Societal Missions—Subproject UPC", Grant PID2021-126436OB-C21, sponsored by MCIN/AEI/10.13039/501100011033/ and EU ERDF "A way to do Europe". The authors are grateful for assistance by the Deltares EFS support team for guidance during the measurement campaign and for H. Volten of RIVM for the use of GroundSPEX.

Author contributions

AdF: conceptualization, analysis, data visualisation, writing of original draft; ME: supervision, interpretation, review & editing; WB: setup and measurements; JF, TC, MV, PM, NL, AM, JC, RC, SM, CF, NF: setup, measurements, and analysis ITP; MDS, AM: setup, measurements, and analysis UoS; EG: technical support measurements UoS; AC, APP, AG: measurements, setup and analysis UPC; OB, SG, SMS: measurements, setup and analysis UoO/L and ITC; QX, RC: measurements, setup and analysis to determine concentration; TvdB: conceptualization advice, measurements, setup and analysis to determine concentration, review & editing; PdM: project initiation, funding and guidance ESA.

Declarations

Competing interests

The authors declare no competing interests.

Additional information

Supplementary Information The online version contains supplementary material available at https://doi.org/10.1038/s41598-024-74332-5.

Correspondence and requests for materials should be addressed to A.F.

Reprints and permissions information is available at www.nature.com/reprints.

Publisher's note Springer Nature remains neutral with regard to jurisdictional claims in published maps and institutional affiliations.

Open Access This article is licensed under a Creative Commons Attribution-NonCommercial-NoDerivatives 4.0 International License, which permits any non-commercial use, sharing, distribution and reproduction in any medium or format, as long as you give appropriate credit to the original author(s) and the source, provide a link to the Creative Commons licence, and indicate if you modified the licensed material. You do not have permission under this licence to share adapted material derived from this article or parts of it. The images or other third party material in this article are included in the article's Creative Commons licence, unless indicated otherwise in a credit line to the material. If material is not included in the article's Creative Commons licence and your intended use is not permitted by statutory regulation or exceeds the permitted use, you will need to obtain permission directly from the copyright holder. To view a copy of this licence, visit http://creativecommons.org/licenses/by-nc-nd/4.0/.

© The Author(s) 2024